Supporting Information

Robust design of Ru quantum dot/N-doped holey graphene for efficient Li-O_2 batteries

Masoud Nazarian-Samani,[1,2] Hee-Dae Lim,[3] Safa Haghighat-Shishavan,[2] Hyun-Kyung Kim,[4] Youngmin Ko,[3] Myeong-Seong Kim,[2] Suk-Woo Lee,[2] Seyed Farshid Kashani-Bozorg,[1,*] Majid Abbasi,[5,6] Hwan-Uk Guim,[7] Dong-Ik Kim,[5] Kwang-Chul Roh,[8] Kisuk Kang,[3,*] Kwang-Bum Kim,[2,*]

[1]School of Metallurgy and Materials Engineering, College of Engineering, University of Tehran, Tehran 11155-4563, IR Iran.

[2]Department of Materials Science and Engineering, Yonsei University, 134 Sinchon-dong, Seodaemoon-gu, Seoul 120-749, Republic of Korea.

[3]Department of Materials Science and Engineering, Research Institute of Advanced Materials (RIAM), Seoul National University (SNU), 1 Gwanak-ro, Gwanak-gu, Seoul 151-742, Republic of Korea.

[4]Department of Materials Science and Metallurgy, University of Cambridge, 27 Charles Babbage Road, Cambridge CB3 0FS, UK.

[5]High Temperature Energy Materials Research Center, Korea Institute of Science and Technology (KIST), Seoul 136-791, Republic of Korea.

[6]Global Technology Center, SK Innovation, Daejeon 305-712, Republic of Korea.

[7]Nano-Bio Electron Microscopy Research Team, Korea Basic Science Institute (KBSI), Daejeon 305-333, Republic of Korea.

[8]Energy Efficient Materials Team, Energy and Environmental Division, Korea Institute of Ceramic Engineering and Technology (KICET), 233-5 Gasan-dong, Guemcheon-gu, Seoul 153-801, Republic of Korea.

* Corresponding authors: fkashani@ut.ac.ir, matlgen1@snu.ac.kr, and kbkim@yonsei.ac.kr

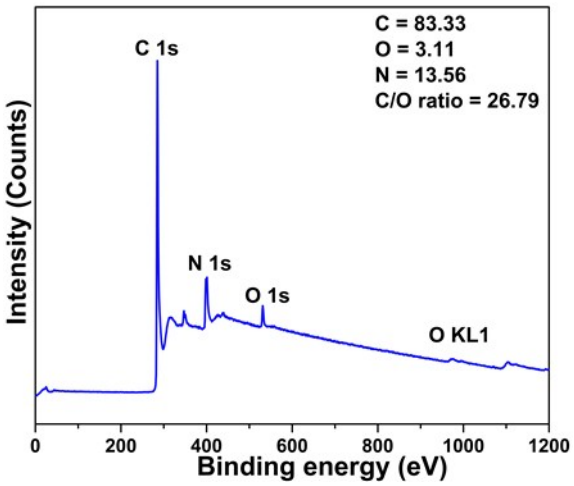

Fig. S1. XPS spectrum of N-doped graphene monolith without Ru QDs.

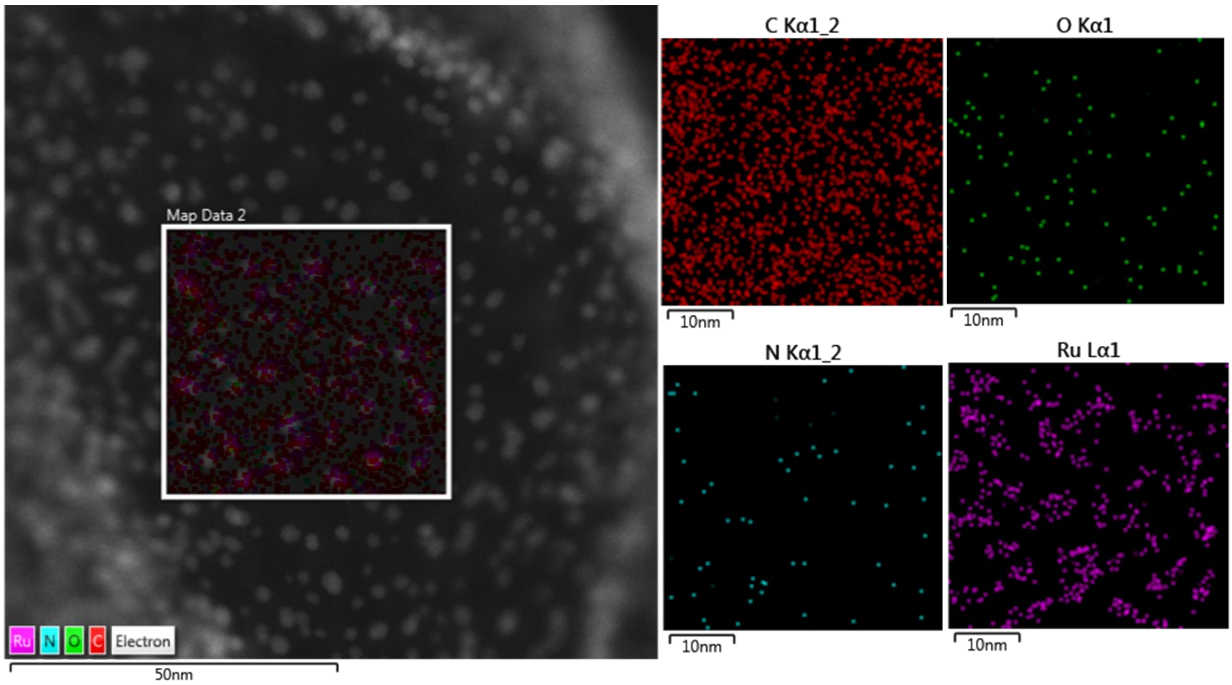

Fig. S2. HAADF-STEM image (left) and EDS mapping of C, O, N, Ru (right) of the Ru QD/NG composite with ~30 wt.% Ru. The Ru mapping result is overlaid in the HAADF-STEM image on the left.

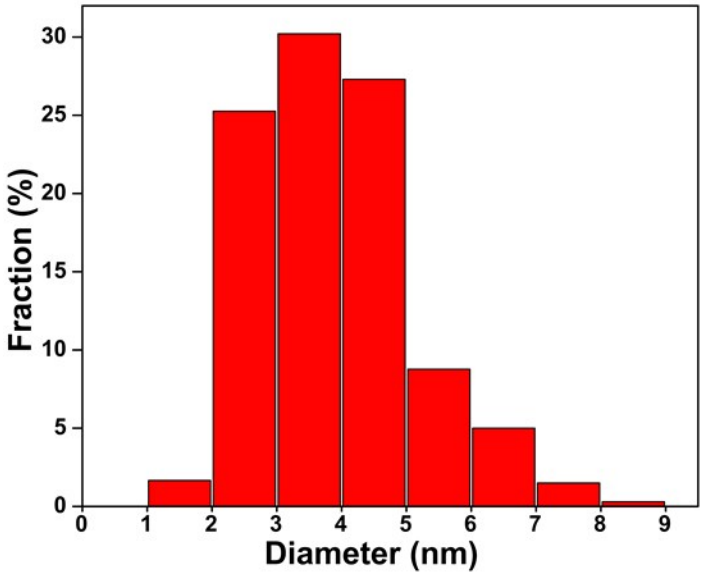

Fig. S3. Ru particle size distribution in the Ru QD/NHG composite after Ar treatment.

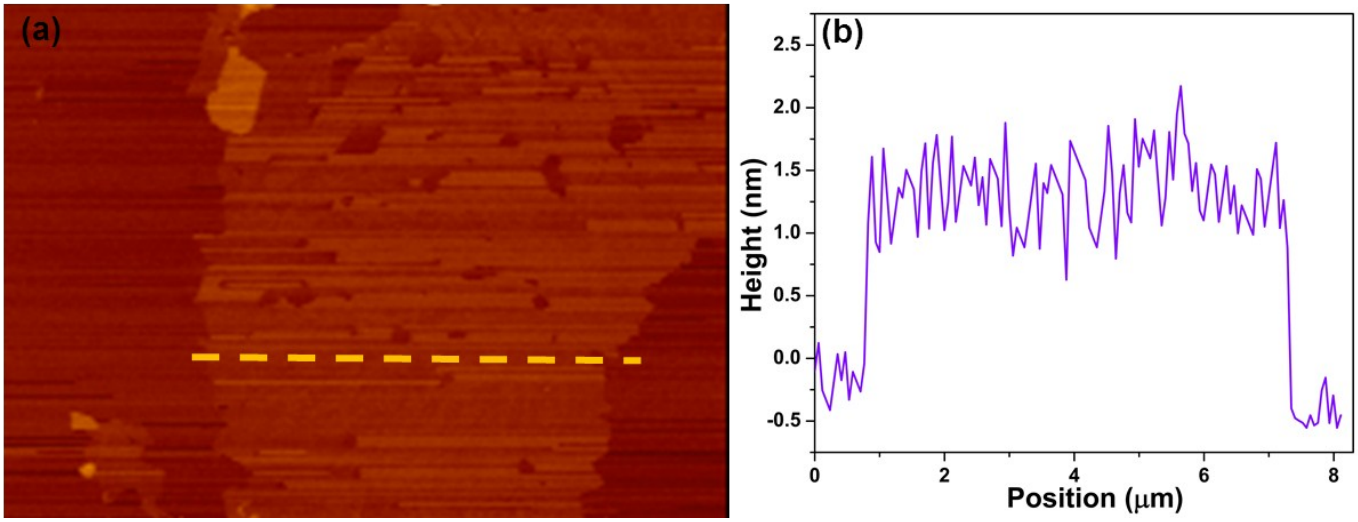

Fig. S4. (a) Sample AFM image of Ar-treated Ru QD/NHG and (b) height profile along the dashed line in panel a. The thickness of the final composite was determined from the average of the step heights at the edges of the graphene sheets.

Table S1. Results of N_2 adsorption/desorption measurements for all the studied samples. (1): Ru QD/NG, (2) acid-treated Ru QD/NHG, and (3) Ar-treated Ru QD/NHG.

Sample	Surface area (m^2/g)	Pore volume (cm^3/g)	BJH pore diameter (nm)
1	540.8	2.675	3.846
2	350.1	1.487	3.829
3	397.8	1.477	3.870

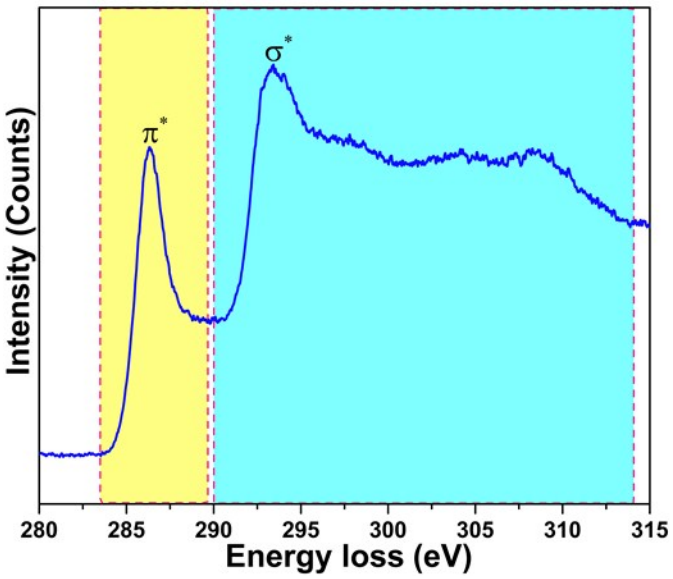

Fig. S5. EELS analysis of graphite, which is considered 100% sp^2 carbon.

The content of sp^2-type carbon was estimated by means of EELS measurements using the following equation:[1]

$$\frac{sp^2}{sp^2+sp^3} = \frac{\frac{I^u_{\pi^*}}{I^u_{\pi^*}+I^u_{\sigma^*}}}{\frac{I^g_{\pi^*}}{I^g_{\pi^*}+I^g_{\sigma^*}}}$$

where I^u and I^g are the integrated peak intensities of the composite and graphite, respectively. Two energy ranges, corresponding to sp^2 and sp^3 hybridized carbon atoms, were considered for calculating the integrated peak intensities: 283.41–289.32 eV for $1s\rightarrow\pi^*$, and 289.98–313.88 eV for $1s\rightarrow\sigma^*$ transitions.

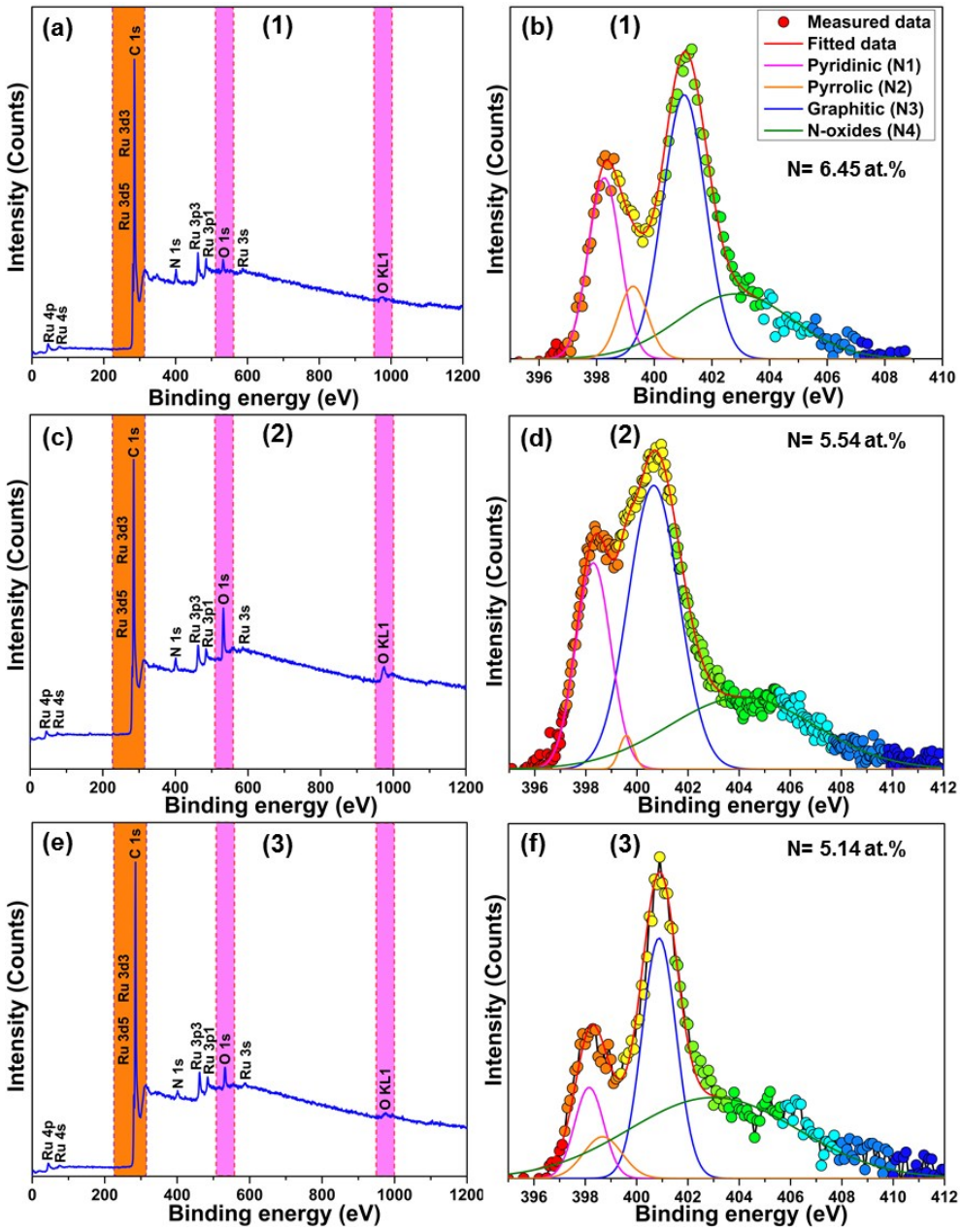

Fig. S6. (a, c, e) Normal XPS and (b,d,f) high-resolution N1s XPS spectra of the following samples. (1) Ru QD/NG, (2) acid-treated Ru QD/NHG, and (3) Ar-treated Ru QD/NHG composites. The content of nitrogen doping is also presented, showing that it was diminished after both the acid treatment and Ar annealing processes.

In the normal scan of the samples, as presented in **Figs. S6 (a, c, e)**, many Ru XPS peaks such as 3s, 3p, 3d, 4s, and 4p are seen, along with the C 1s, N 1s, O 1s and O KL1 peaks indicating the existence of the respective elements in the composite. The content of nitrogen in the Ru QD/NG was estimated to be 6.45 at.%, in agreement with the EDS/TEM as well as EA measurements. However, after acid treatment and after Ar annealing this content was reduced to 5.54 and 5.14 at.%, respectively. The N 1s high-resolution XPS peak in **Fig. S6** indicates the existence of four nitrogen species: pyridinic (lattice of graphene, N1), pyrrolic (N2), graphitic contribution (in-plane insertion, N3), and pyridinic oxide (N4).[2] It is evident from **Figs. S6 (b, d, f)** that the contribution of N3 nitrogen atoms is more than the others in all three samples, since the pyridinic type is located on the edges and therefore unstable during the subsequent treatments. The graphitic type, which is inserted into the graphene structure as in-plane introduction, remains stable through the graphene sheets. The high-temperature Ar annealing also confirms the highest thermal stability of the N3 type. The existence of N-oxides can be attributed to the oxidizing environment during the acid treatment in the second step. The co-existence of pyrrolic/graphitic nitrogen types could generate more active sites for higher OER activity, while providing an effective chemical interconnection for rapid electron transfer.

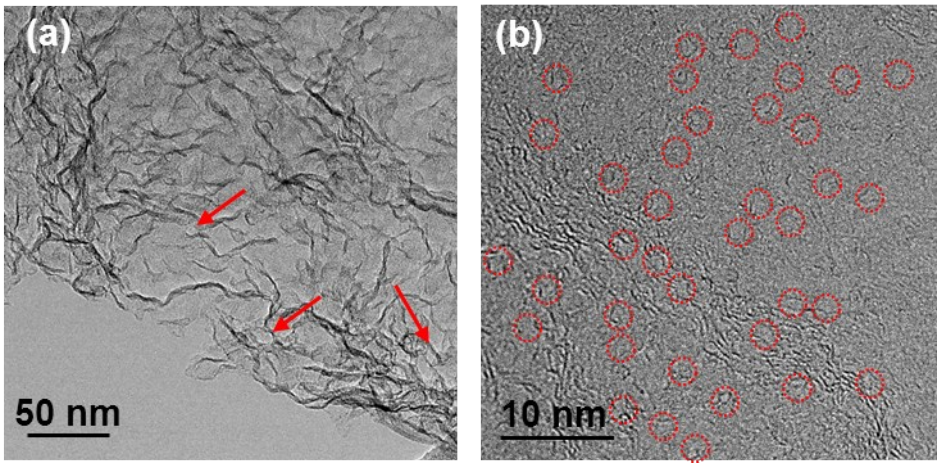

Fig. S7. TEM images of the bare acid-treated NHG at (a) low and (b) high magnifications. Both the arrows and red circles indicate the in-plane nanopores, clearly confirming the importance of Ru QDs for the creation of large in-plane holes.

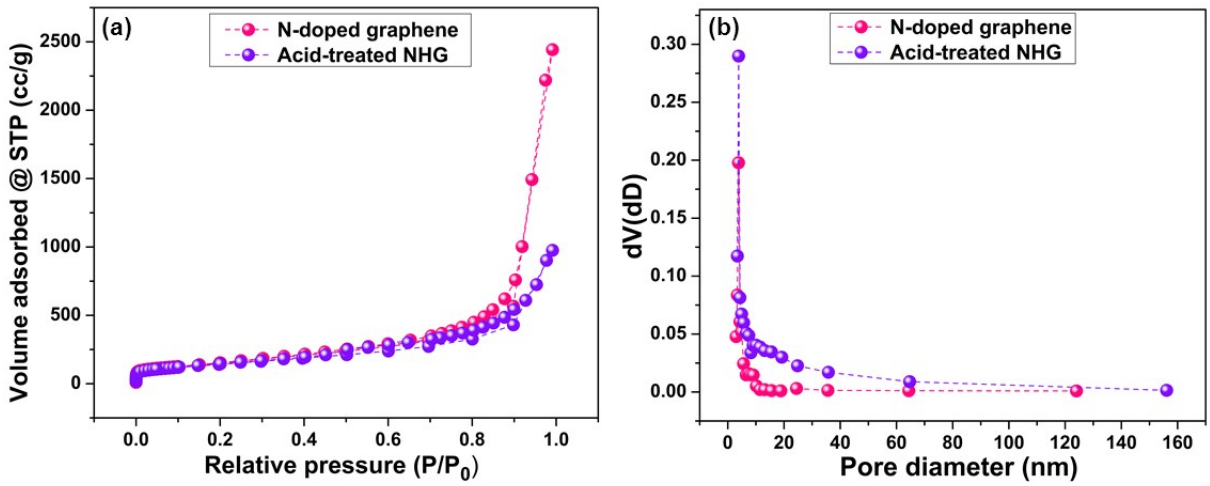

Fig. S8. (a) N_2 adsorption/desorption isotherms, and (b) BJH pore size distributions of NG and acid-treated NHG. As explained in the main manuscript, the high power and long bath sonication plus acid treatment break the graphene sheets, thereby reducing the BET surface area (from 550.9 $m^2 g^{-1}$ in NG to 512.4 $m^2 g^{-1}$ in the acid-treated NHG sample).

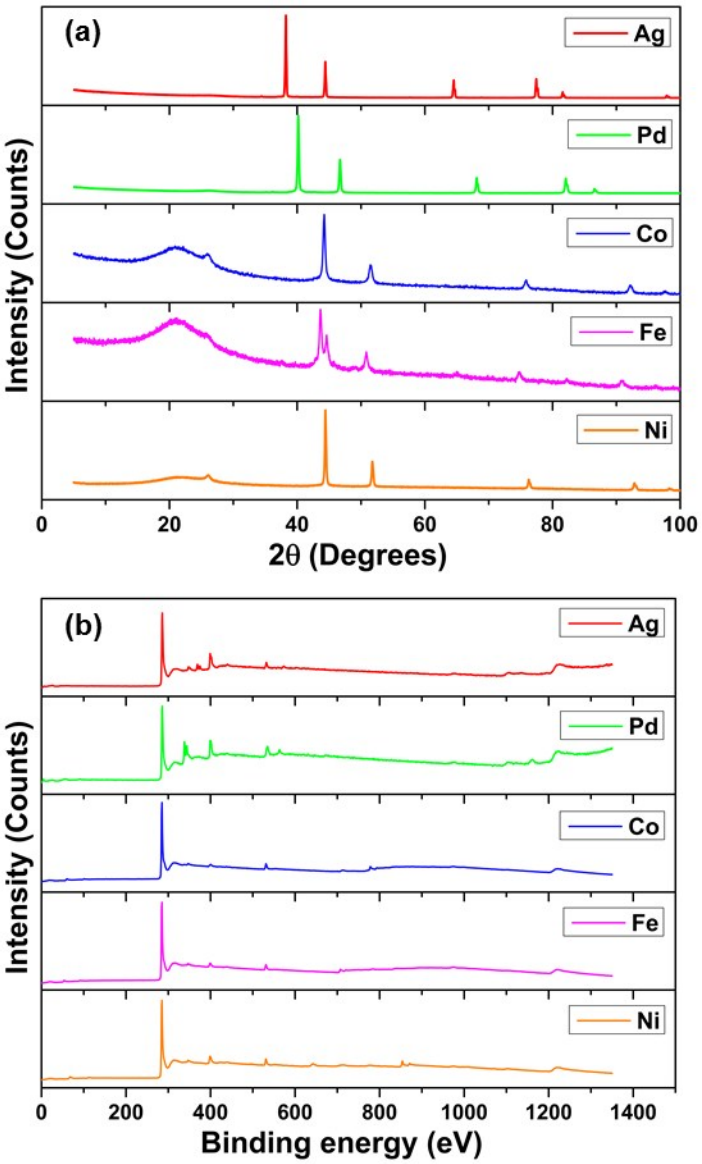

Fig. S9. (a) XRD patterns and (b) normal XPS spectrum of M/NG (M = Ag, Pd, Co, Fe, or Ni) composites using the method described in Scheme 1.

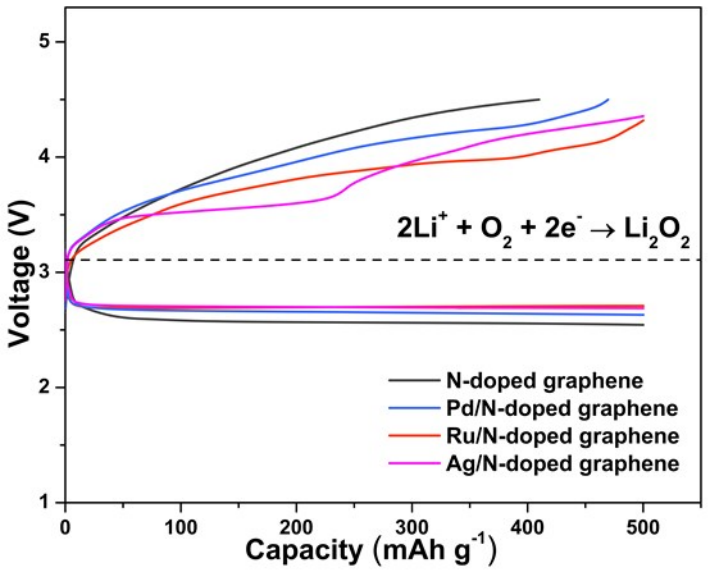

Fig. S10. Comparison of the first charge-discharge cycle of different M/NG electrodes, with a limited discharge capacity of 500 mAh g^{-1} and at a constant current of 300 mA g^{-1}. It is evident that the Ru QDs led to the most stable performance in terms of lowered charge overpotentials.

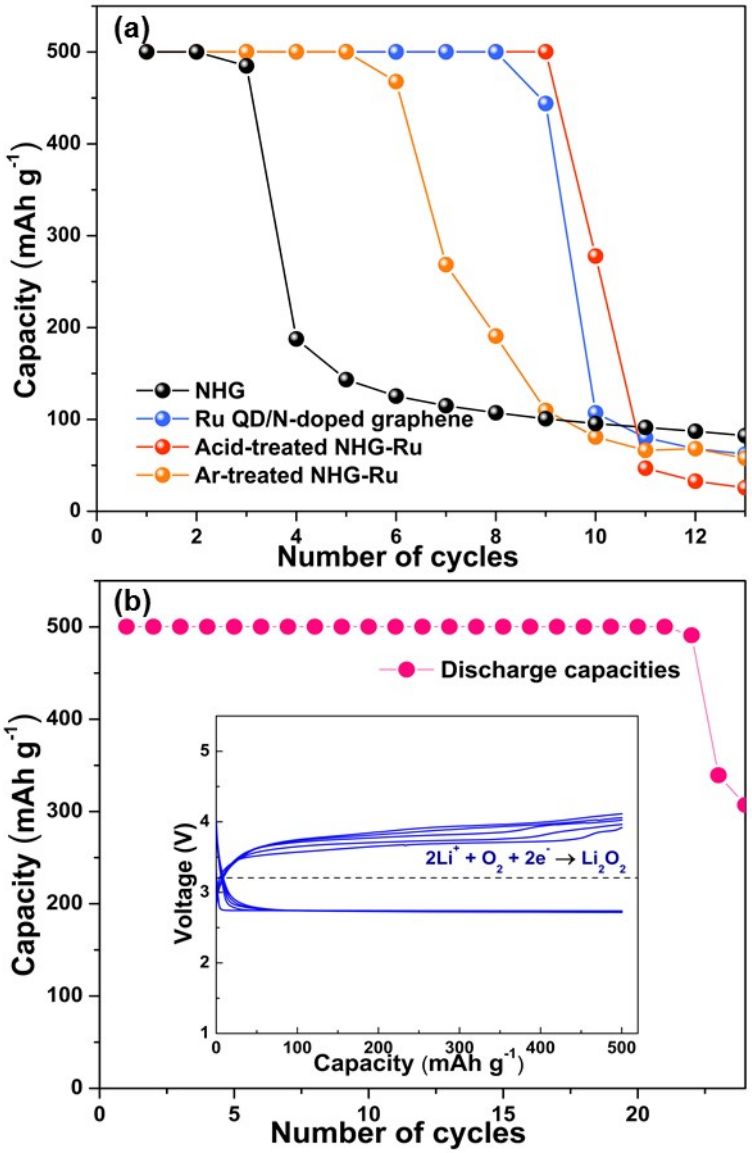

Fig. S11. (a) Comparison of the cyclic performance of bare NHG, Ru QD/NG, acid-treated Ru QD/NHG, and Ar-treated Ru QD/NHG electrodes. (b) Cyclic performance of acid-treated Ru QD/NHG using the electrolyte of $LiNO_3$ in DMA. Inset: initial 5 cycles of acid-treated Ru QD/NHG electrode using $LiNO_3$-DMA electrolyte.

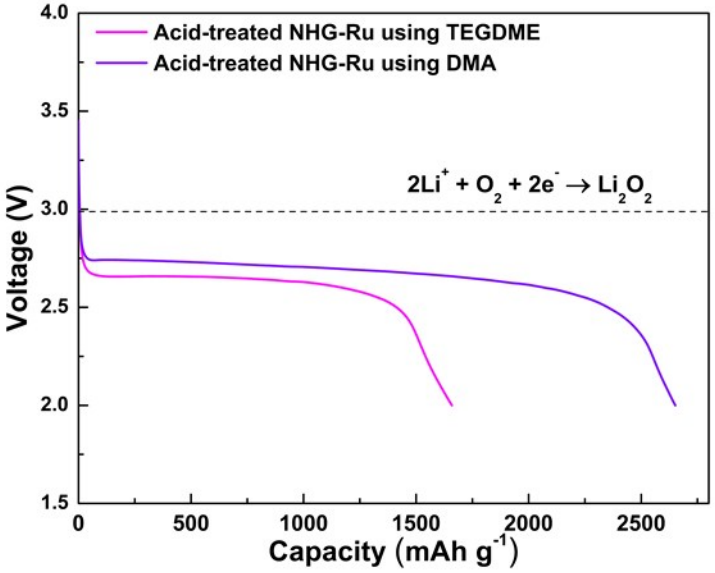

Fig. S12. Discharge profiles of acid-treated Ru QD/NHG electrode when using TEGDME and DMA electrolytes, at a constant rate of 300 mA g^{-1} with a full discharge to 2.0 V.

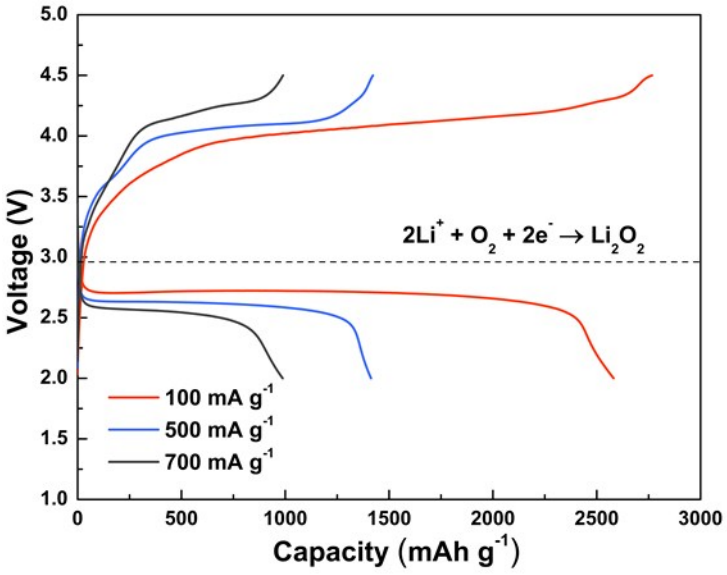

Fig. S13. Electrochemical profiles of acid-treated Ru QD/NHG electrode at the various current rates of 100, 500, and 700 mA g^{-1} with a full discharge to 2.0 V.

Electrochemical profiles of the acid-treated Ru QD/NHG electrode were acquired at various current rates with a full discharge and charge between 2.0 and 4.5 V. It should be noted that the charge polarization did not decrease sharply compared to that of the cell with capacity-limited mode, as shown in **Fig. 4c**. The discharge capacity decreased with increasing current rate, mainly due to the formation of non-conductive solid discharge products (has been demonstrated later using SEM images) when the cell was fully discharged to 2.0 V. These solid products consequently hindered the functioning of the solid catalyst (**Fig. S13**).

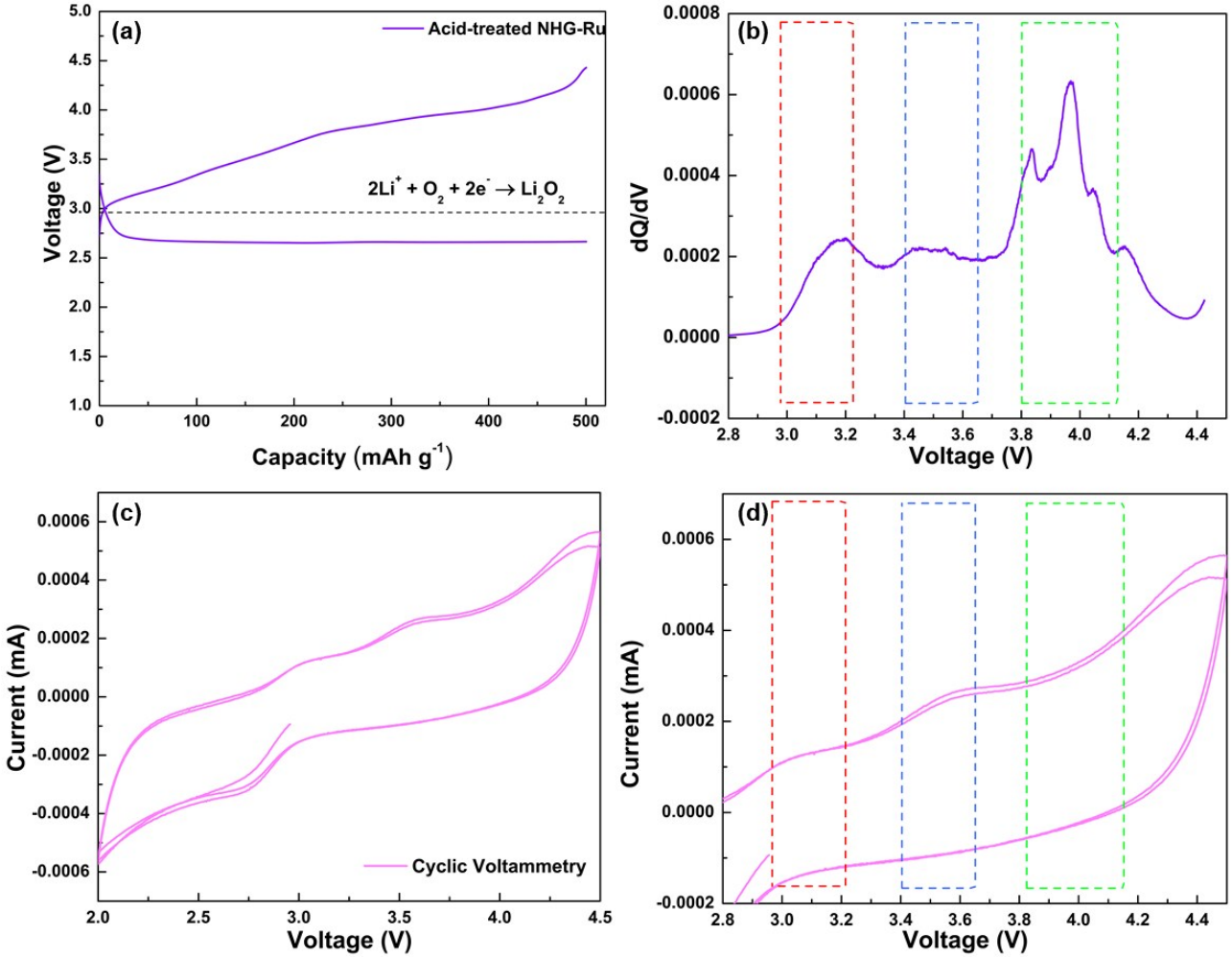

Fig. S14. (a) First discharge-charge graph of acid-treated Ru QD/NHG electrode, and the corresponding (b) the dQ/dV charge curve. (c) CV curves of acid-treated Ru QD/NHG electrode using a three-electrode cell at a constant rate of 5 mV s^{-1}. (d) Enlarged right-side portion of (c).

Table S2. Electrochemical performance data of Li-O_2 batteries containing Ru electrocatalysts from recent literatures.

Material	Round-trip efficiency (%) (current density)	Ave. charge voltage (V)	Ave. discharge voltage (V)
Ru QD/NHG (**This work**)*	75 (300 mA g^{-1})	3.60	2.70
Ru+RuO_2.0.64H_2O/rGO[3]	75 (200 mA g^{-1})	3.70-3.90	2.70
Ru-rGO[4]	76 (200 mA g^{-1})	3.50	2.71
Ru@CNT[5]	71 (500 mA g^{-1})	3.76	2.71
Hierarchical Ru spheres[6]	76 (200 mA g^{-1})	3.52	2.76
Ru@porous graphene[7]	80 (200 mA g^{-1})	3.54	2.79
Ru vertical graphene@Ni[8]	78 (200 mA g^{-1})	3.50	2.79

*Parameters are based on the limited mode in a discharge capacity of 500 mAh g^{-1} and at a constant current of 300 mA g^{-1}. The data from literature were also obtained in limited modes to enable better comparison.

According to the data in Table S2, the acid-treated Ru QD/NHG cell in a limited mode delivered an energy efficiency of 75% in the 1st cycle (consistent with **Fig. 4b**), which is comparable to that of other recently reported Ru electrocatalysts. The average charge and discharge voltages are 3.60 and 2.70 V, respectively. In addition, the cell could deliver an energy density of 1350 Wh kg^{-1} and a power density of 810 W kg^{-1} in the same limited mode condition. The energy and power densities for full discharge to 2.0 V, which were calculated based on **Fig. S12**, are 4283 Wh kg^{-1} and 775 W kg^{-1} for TEGDME electrolyte, and 7000 Wh kg^{-1} and 792 W kg^{-1} for DMA one, respectively.

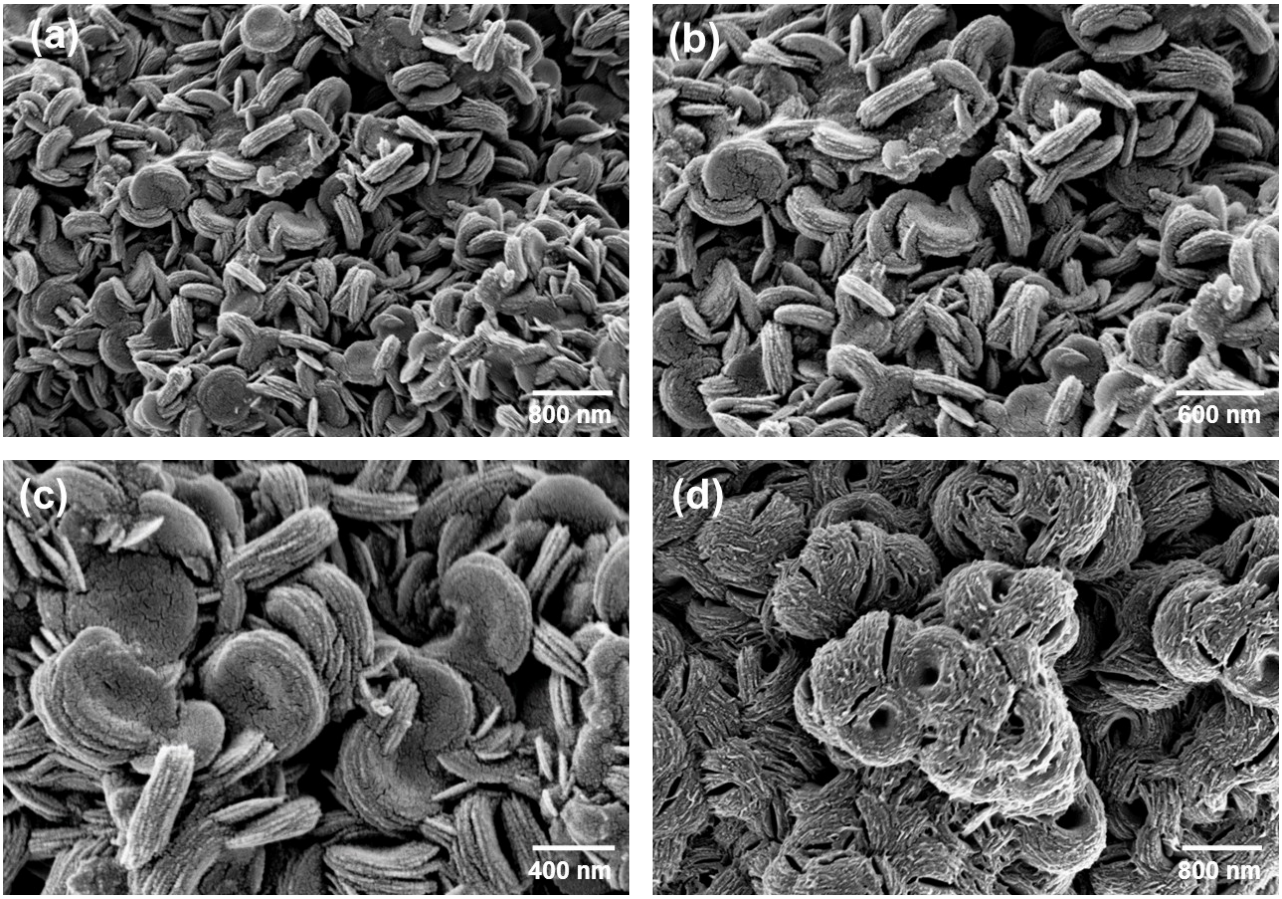

Fig. S15. SEM images of the acid-treated Ru QD/NHG electrode after the first full discharge to 2.0 V using (a, b, c) TEGDME and (d) DMA electrolytes.

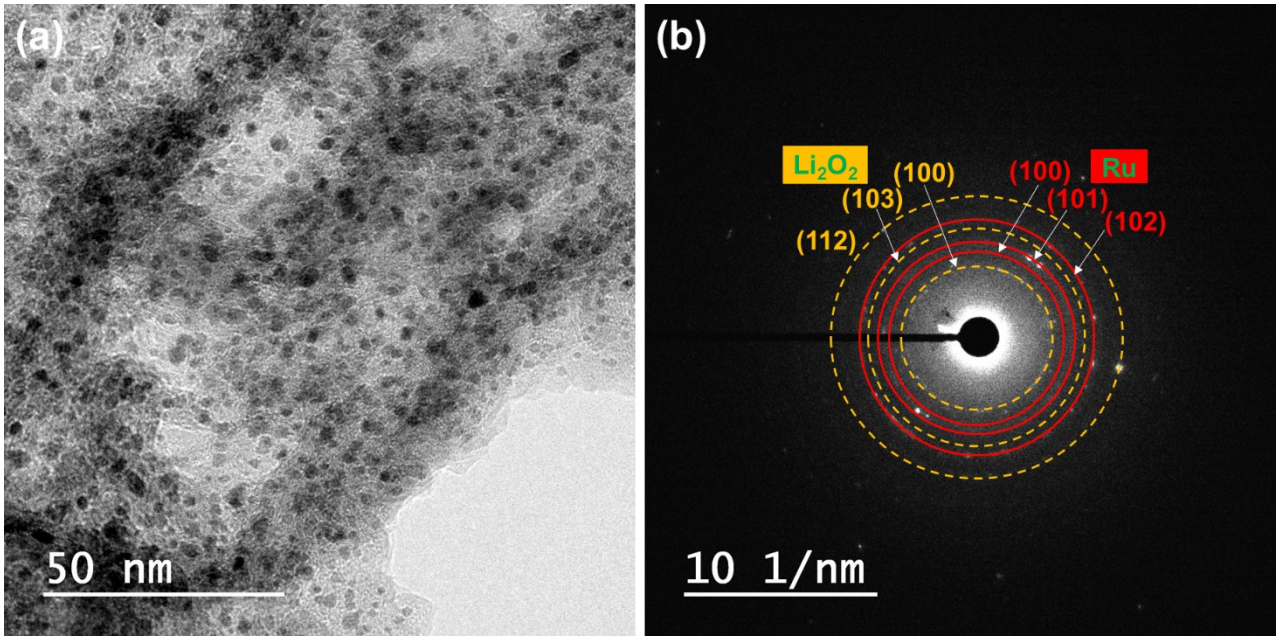

Fig. S16. TEM micrograph and the corresponding SAED pattern of the acid-treated Ru QD/NHG after the first full discharge to 2.0 V, demonstrating the formation of Li_2O_2 after the discharge process.

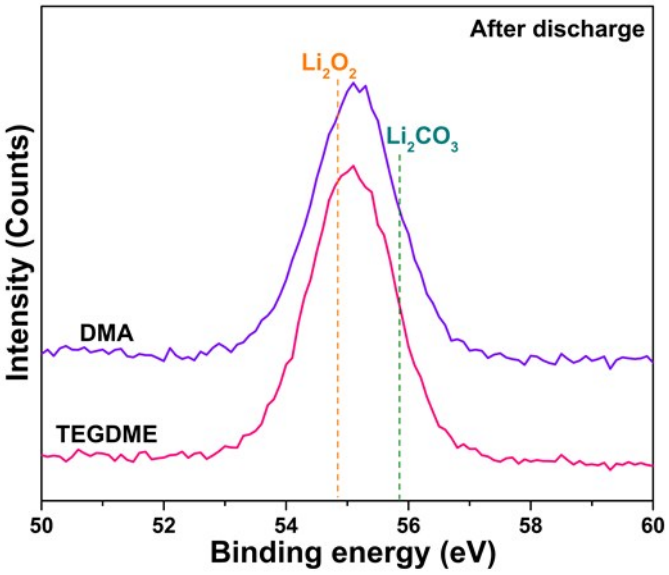

Fig. S17. Comparison of Li 1s XPS spectra of the acid-treated Ru QD/NHG using (a) TEGDME and (b) DMA electrolytes, after the first full discharge to 2.0 V.

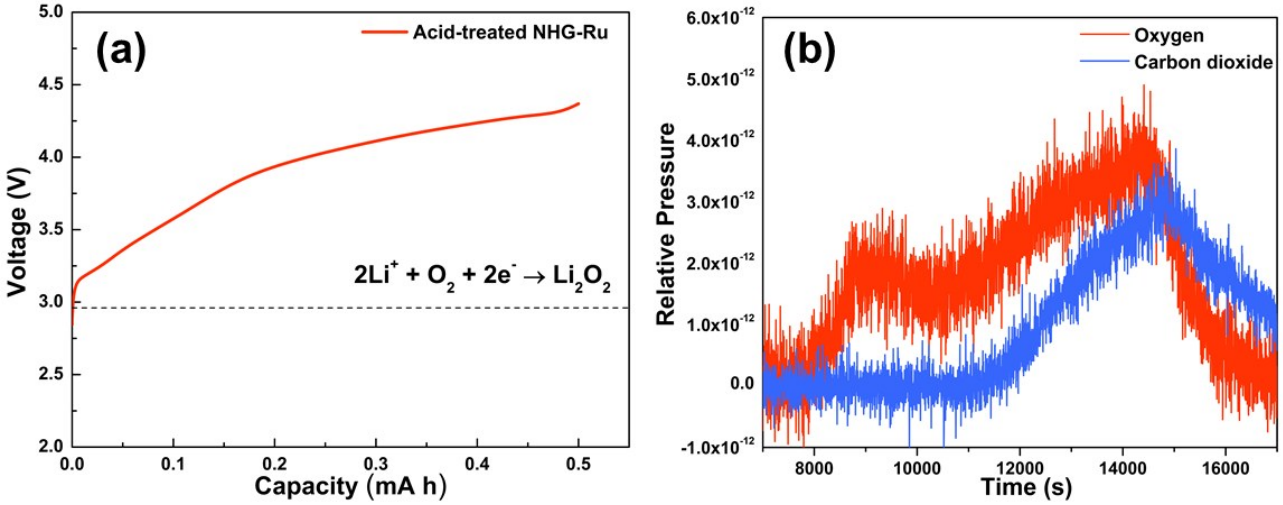

Fig. S18. (a) Charge profile of the acid-treated Ru QD/NHG electrode with the limited capacity of 0.5 mA h, and (b) the related gas evolution profile obtained using *in-situ* DEMS analysis.

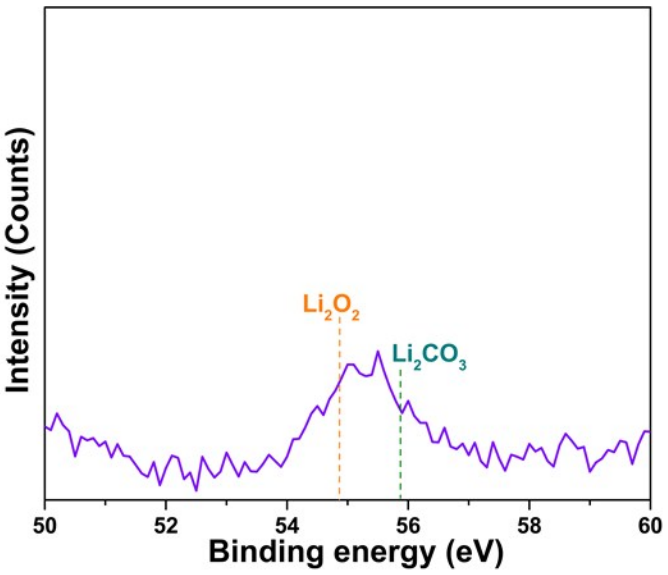

Fig. S19. Li 1s XPS spectra of the acid-treated Ru QD/NHG electrode after cycling.

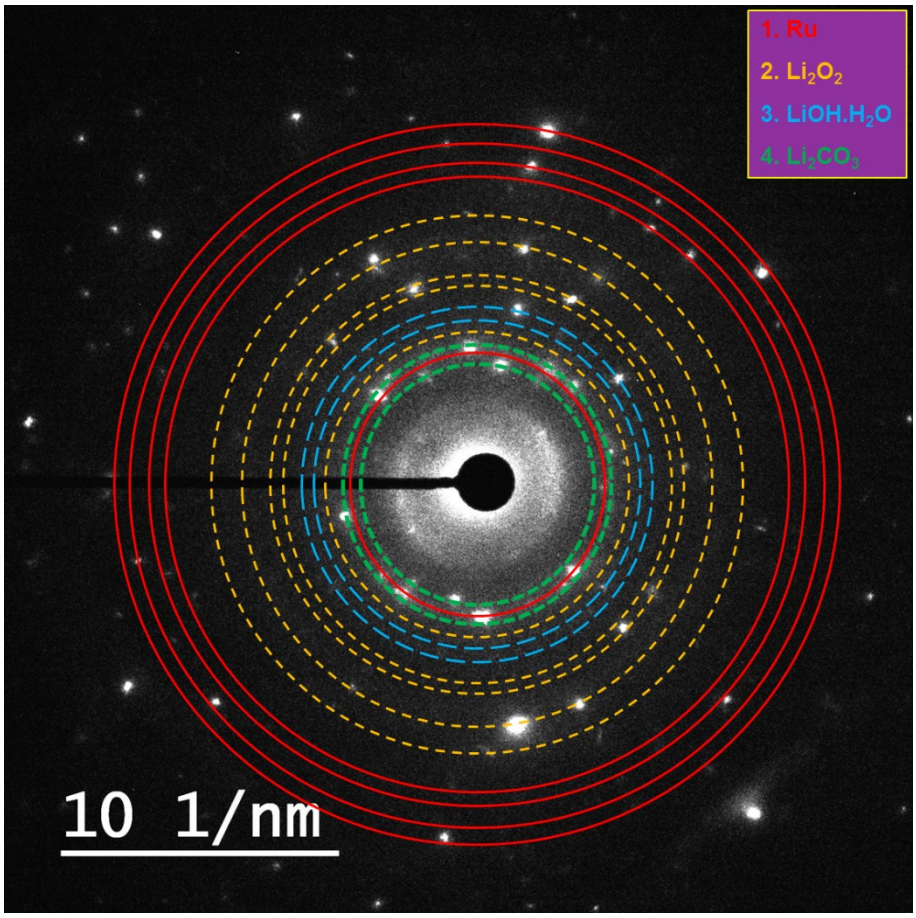

Fig. S20. SAED pattern of acid-treated Ru QD/NHG electrode after cycling, demonstrating the formation of Li_2CO_3 and $LiOH \cdot H_2O$ by-products along with Ru QDs and the Li_2O_2 phase.

Supporting References

1 Y. Zhu, S. Murali, M. D. Stoller, K. J. Ganesh, W. Cai, P. J. Ferreira, A. Pirkle, R. M. Wallace, K. A. Cychosz, M. Thommes, D. Su, E. A. Stach and R. S. Ruoff, *Science*, 2011, **332**, 1537–1541.

2 Y. Shao, S. Zhang, M. H. Engelhard, G. Li, G. Shao, Y. Wang, J. Liu, I. A. Aksay and Y. Lin, *J. Mater. Chem.*, 2010, **20**, 7491-7496.

3 H. G. Jung, Y. S. Jeong, J. B. Park, Y. K. Sun, B. Scrosati and Y. J. Lee, *ACS Nano*, 2013, **7**, 3532–3539.

4 Y. S. Jeong, J.-B. Park, H.-G. Jung, J. Kim, X. Luo, J. Lu, L. Curtiss, K. Amine, Y.-K. Sun, B. Scrosati and Y. J. Lee, *Nano Lett.*, 2015, **15**, 4261–4268.

5 F. Li, Y. Chen, D.-M. Tang, Z. Jian, C. Liu, D. Golberg, A. Yamada and H. Zhou, *Energy Environ. Sci.*, 2014, **7**, 1648–1652.

6 D. W. Su, S. X. Dou and G. X. Wang, *J. Mater. Chem. A*, 2015, **3**, 18384–18388.

7 B. Sun, X. Huang, S. Chen, P. Munroe and G. Wang, *Nano Lett.*, 2014, 14, 3145–3152.

8 D. Su, D. Han Seo, Y. Ju, Z. Han, K. Ostrikov, S. Dou, H.-J. Ahn, Z. Peng and G. Wang, *NPG Asia Mater*, 2016, **8**, e286.